Mapping H_2 Excitation and Mass across M51 with the Spitzer Infrared Spectrograph

Gregory Brunner[1,2]

Department of Physics and Astronomy, Rice University,

Houston, TX 77005

gbrunner@ipac.caltech.edu, gbrunner@rice.edu

Kartik Sheth[3], Lee Armus[3], and George Helou[3]

Spitzer Science Center, Pasadena, CA 91125

Eva Schinnerer[4]

Max-Planck-Intitüt für Astronomie, Heidelberg, Germany

Stuart Vogel[5] and Mark Wolfire[5]

Department of Astronomy, University of Maryland, College Park, MD 20741

and

Reginald Dufour[1]

Department of Physics and Astronomy, Rice University, Houston, TX 77005

Received ______________________; accepted ______________________

[1]Department of Physics and Astronomy, Rice University, Houston, TX 77005

[2]Visiting Graduate Student Fellow, Spitzer Science Center, Caltech, Pasadena, CA 91125

[3]Spitzer Science Center, Caltech, Pasadena, CA 91125

[4]Max-Planck-Institüt für Astronomie, Heidelberg, Germany

[5]Department of Astronomy, University of Maryland, College Park, MD 20741

ABSTRACT

We have mapped the H_2 S(0) $-$ H_2 S(5) pure rotational lines over a strip across M51 using the *Spitzer Space Telescope* Infrared Spectrograph. We find that the molecular gas morphology of M51 varies through each line. We use the H_2 maps to model the H_2 excitation-temperature and mass across the galaxy and find that the H_2 exists in a continuous distribution of temperatures from 100 $-$ 1000 K. Using the low J lines to trace the warm (T = 100 $-$ 300 K) H_2, we find that the warm H_2 excitation-temperature is highest in the nuclear region (192 K) and lower within the spiral arms (150 $-$ 170 K). Using the higher J lines to trace the hot (T = 400 $-$ 1000 K) H_2, we find that the hot H_2 excitation-temperature is lowest in the inner spiral arms (500 $-$ 550 K) and increases to $\sim$ 600 K in the nucleus, where the largest hot H_2 mass densities are found (0.24 $M_\odot/pc^2$). The warm-to-hot H_2 mass ratio is not constant across the galaxy indicating different primary excitation mechanisms for the warm and hot H_2 phases. We compare H_2 to CO (J = 1 $-$ 0) emission and find offsets between the warm and hot H_2 mass phases and the CO. One possible explanation for the offsets between the warm H_2 mass and CO is that the warm H_2 traces the sites of active star formation within the molecular clouds. We compare H_2 to Hα emission and find the warm and hot H_2 mass are located in the Hα dust lanes with the one exception being the inner spiral arms where the warm H_2 mass coincides with Hα emission. In the nuclear region, the hot H_2 is coincident with [O IV](25.89 μm) emission and X-ray emission suggesting that shocks and X-rays are the dominant excitation mechanisms of the hot H_2 phase.

Subject headings: galaxies: ISM — galaxies: H_2 — galaxies: individual(M51)

1. Introduction

Star formation and galactic evolution are linked via the molecular gas within a galaxy. In the Milky Way, nearly all star formation occurs in molecular clouds (Blitz 1995), although not all molecular clouds are actively forming stars. In galaxies star formation is triggered whenever the molecular gas surface density is enhanced, for example, by a spiral density wave (Vogel et al. 1988), by increased pressure or density in galactic nuclei (Young and Scoville 1991; Sheth et al. 2005), due to the hydrodynamic shock along the leading edge of bars (Sheth et al. 2000; Sheth et al. 2002), and in the transition region at the ends of bars (Kenny and Lord 1991). Although the connection between star formation and molecular gas is well-established, the exact mechanisms for initiating, controlling, and inhibiting star formation are not well-understood.

M51 (the Whirlpool galaxy, NGC 5194) is a nearby, face-on spiral galaxy that is rich in molecular gas. Its proximity [assumed to be 8.2 Mpc (Tully 1988)], face-on orientation, and grand-design spiral morphology make it an ideal target for studies of the ISM across distinct dynamical, chemical, and physical environments in a galaxy. Studies of the molecular gas within M51 have revealed giant molecular associations (GMAs) along the spiral arms (Aalto et al. 1999), a reservoir of molecular gas associated with the nuclear AGN (Scoville et al. 1998), and star-formation in molecular clouds triggered by a spiral density wave (Vogel et al. 1988). In addition to being well-studied at millimeter and radio wavelengths, M51 has been studied in X-rays, UV, optical, near-infrared, infrared, and submillimeter wavelengths (Palumbo et al. 1985**?** ; Scoville et al. 2001; Calzetti et al. 2005; Matsushita et a. 2004).

The Infrared Spectrograph (IRS) (Houck et al. 2004) on-board the *Spitzer Space Telescope* is a powerful tool for observing the warm (T = 100 − 300 K) and hot (T = 400 − 1000 K) molecular gas within galaxies. The *Spitzer* IRS low resolution modules cover 5 - 38 μm (short-low, SL, 5 - 14 μm; long-low, LL, 14 - 38 μm) giving observers access to the lowest pure rotational H_2 lines with the low J lines tracing the warm molecular gas phase and the higher J lines tracing the hot molecular gas phase. These lines are important diagnostics of the ISM that allow us to model the H_2 excitation-temperature, mass (Rigopoulou et al. 2002; Higdon et al. 2006), and ortho-to-para ratio (Neufeld et al. 1998; Neufeld et al. 2006). By understanding the pure rotational H_2 line emission from a galaxy, constraints can be placed on the energy injection mechanisms (i.e. radiative heating, shocks, turbulence) that heat the warm molecular gas phase in the ISM.

In this paper we present maps of the extinction-corrected H_2 S(0) $-$ H_2 S(5) line intensities over a strip across M51(§3.1) and use the maps to model the warm and hot H_2 excitation-temperature and mass across the galaxy (§3.2). We seek to understand whether the warm and hot phases undergo excitation via the same processes and discern the primary excitation mechanism of H_2 across the galaxy by comparing H_2 to CO ($J = 1 - 0$), Hα, [O IV](25.89 μm) intensity, and X-rays (§4).

2. Observations and Data Reduction

2.1. Spectral Data

We mapped a radial strip across M51 using the short-low (SL) and long-low (LL) modules of the *Spitzer* IRS in spectral mapping mode. The radial strips were $324'' \times 57''$ and $295'' \times 51''$ in the SL and LL, respectively. Integration times in the SL and LL were 14.6 s. Each slit position was mapped twice and half-slit spacings were used. In total, 1,412 spectra were taken in the SL and 100 were taken in the LL (including background observations). Dedicated off source background observations were taken for the SL observations. Backgrounds for the LL observations were taken from outrigger data collected while the spacecraft was mapping in the adjacent module. The astronomical observation requests (AORs) are available on SST's Leopard and Spot (Project ID 200138, PI: K. Sheth).

The spectra were assembled from the basic calibration data (BCD) into spectral data cubes for each module using CUBISM (Kennicutt et al. 2003; Smith et al. 2004). Background subtraction and bad pixel removal was done within CUBISM. The individual IRS spectra were processed using the S14.0 version of the Spitzer Science Center (SSC) pipeline. In CUBISM, the SL and LL data cubes have resolutions of 1.85″/pixel and 5.08″/pixel, respectively. The spatial resolution of the data cubes varies as a function of wavelength from 1$''\!.$85 at 5.2 μm to 13$''\!.$8 at 38 μm.

We created maps of the H_2 S(0) − H_2 S(5) lines with PAHFIT (Smith et al. 2007), a spectral fitting routine that decomposes IRS low resolution spectra. The advantage of using PAHFIT is that it allows the recovery of the full line flux of blended H_2 lines such as H_2 S(1), blended with the 17.0 μm PAH complex; H_2 S(2), blended with [Ne II](12.8 μm); and H_2 S(5), blended into [Ar II](6.9 μm). We ran PAHFIT through the SL (SL1 + SL2) and LL (LL1+ LL2) cubes separately. The concatenated SL and LL data cubes were each smoothed spatially by a 3 × 3 pixel box prior to running PAHFIT to increase the signal-to-noise ratio of the spectra. When running PAHFIT through the SL and LL data cubes we measured the extinction-corrected line intensity of every spectral line in the data cubes while saving the information about the position (RA and Dec) of each spectrum and in doing so, we constructed line-intensity maps.

2.2. Ancillary Data: CO Map, Hα Imagery, and X-ray Observations

The BIMA (Berkely Illinois Maryland Array) CO (J = 1 − 0) map was acquired as a part of the BIMA Survey of Nearby Galaxies (SONG) (Regan et al. 2001; Helfer et al. 2003). The beam size is $5''.8 \times 5''.1$ (220 pc × 190 pc).

The Hα + [N II] image of M51 was observed at Kitt Peak as part of the *Spitzer Infrared Nearby Galaxies Survey* (SINGS). The pixel scale is $0''.305$ and the flux scale is in counts/sec. Additional information about the Hα image can be found in the SINGS Fourth Data Release (DR4).

X-ray emission from M51 was observed by the Advanced CCD Imaging Spectrometer (ACIS) on the *Chandra X-Ray Observatory* on 20 June 2000. The total integration time was 14,865 seconds. The resolution of the image is $\sim 1''$. Further details of the observations are presented in (Terashima and Wilson 2001).

3. Results

3.1. Morphology of H_2 Emission

We have detected and mapped H_2 emission from the six lowest pure rotational H_2 lines (Figure 1). The maps of H_2 line intensity reveal remarkable differences in the morphology of M51 through each line. H_2 S(0) emission is strongest in the northwest spiral arm peaking at an intensity of 3.66×10^{-18} W/m^2 and decreases by a factor of 2 in the nuclear region. The H_2 S(1) emission peaks in the nucleus of the galaxy at an intensity of 1.03×10^{-17} W/m^2 and shows similar intensity moving into the northwest spiral arm. The peaks in H_2 S(0) and H_2 S(1) emission within the arms are not aligned, they are offset by $10''.2$ (380 pc). These offsets are not a result of the difference in resolution between the two maps, but appear to be real. H_2 S(0) and H_2 S(1) emission is resolved out to 5 − 6 kpc from the nucleus of the galaxy in the northwest outer spiral arm. In the outer spiral arm, the H_2 S(0) intensity is a factor of 2 times lower than in the inner northwest spiral arm and the H_2 S(1) intensity is a factor of 5 times lower than in the nucleus of M51.

The H_2 S(2) − H_2 S(5) maps show different molecular gas morphology within M51 through each H_2 line. The strongest H_2 S(2) emission is from the nuclear region peaking at 2.21×10^{-18} W/m^2. We also see bright H_2 S(2) emission from the inner northwest spiral arm; however, the intensity is a factor of 2 lower than in the nucleus. The H_2 S(3) line exhibits similar strong emission in the nuclear region. The H_2 S(3) intensity in the nucleus is 1.35×10^{-17} W/m^2 which is a factor of ~ 6 greater than the intensity of H_2 S(2) nuclear emission. We see an apparent bar structure in H_2 S(3) emission across the nucleus of the galaxy going north-to-south. We see offsets in the intensity peaks within the spiral arms between the H_2 S(2) and H_2 S(3) maps. An example of this is in the northwest inner spiral arm. In H_2 S(2) emission, we see bright (1.30×10^{-18} W/m^2) H_2 emission to the north of the nucleus. The H_2 S(2) intensity decreases to 7.00×10^{-19} W/m^2 moving southwest in the spiral arm. In the H_2 S(3) emission map, we see the H_2 S(3) intensity increasing from 4.00×10^{-18} W/m^2 to 5.10×10^{-18} W/m^2 as we move from north of the nucleus (the end of the bar structure) to the southwest in the inner spiral arm. The offsets in the peak emission of the H_2 lines are real and indicate variations in the excitation-temperature in each region.

The H_2 S(4) and H_2 S(5) lines are faint across the disk of the galaxy but both are very strong in the nuclear region. In the nucleus, the H_2 S(4) intensity is 3.05×10^{-18} W/m^2 and the H_2 S(5) intensity is 8.04×10^{-18} W/m^2. H_2 S(5) emission is asymmetric in the nucleus and mimics the morphology of the H_2 S(3) line with extended emission to the north of the nucleus. The H_2 S(4) line shows emission in the nucleus and in the spiral arm to the west. In the spiral arm to the west of the nucleus, the H_2 S(4) intensity is 2.11×10^{-18} W/m^2. This is notable because the spiral arm to the southwest of the nucleus is very bright in CO and and studies have revealed very high molecular gas column densities in the southwest inner spiral arm (Lord and Young 1990). The differences in the morphology of H_2 emission are indicative of changes in the H_2 excitation-temperature across the galaxy, which we discuss in the next section.

3.1.1. Note on Uncertainties in the H_2 *Line Intensity Maps*

The uncertainty in the H_2 line intensity varies as a function of line intensity across each map. The uncertainty in the H_2 S(0) line intensity ranges from 20 − 40 % across the nuclear region and spiral arms. The uncertainty in the spiral arm intensity at greater distances from the center of the strip is 80 − 90 %. The H_2 S(1) line map has lower uncertainties with the uncertainty being $\sim$ 10 % in the nuclear region and 20 − 30 % in the spiral arms. The H_2 S(2) and H_2 S(3) lines show similar uncertainties to each other. In the nuclear region their uncertainty is 10 − 30 % and in the spiral arms their uncertainty is 50 − 80 %. The H_2 S(4) and H_2 S(5) lines only show emission from the nuclear region; their uncertainties in the line intensity are $\sim$ 35 % and 25 %, respectively.

3.2. Mapping H_2 Excitation-Temperature and Mass across M51

3.2.1. Modeling H_2 *Excitation-Temperature and Mass*

The pure rotational lines of molecular hydrogen provide a powerful probe of the conditions of the ISM and place constraints on the energy injection processes that excite H_2 (Neufeld et al. 2006). From the maps of H_2 S(0) − H_2 S(5) emission, we have modeled the H_2 excitation-temperature and mass (Rigopoulou et al. 2002; Higdon et al. 2006) across

M51.

In order to model the H_2 excitation and mass across the galaxy, the H_2 S(1) − H_2 S(5) maps were smoothed to the resolution of the H_2 S(0) map. The maps were then interpolated to the same spatial grid. Excitation diagrams across the strip were derived from the Boltzman equation using the formulation from Rigopoulou et al. (2002),

$$N_i/N = (g(i)/Z(\mathrm{T_{ex}}))exp(-T_i/\mathrm{T_{ex}}) \tag{1}$$

where $g(i)$ is the statistical weight of state i, $\mathrm{Z(T_{ex})}$ is the partition function, $\mathrm{T_i}$ is the energy level of a given state, and $\mathrm{T_{ex}}$ is the excitation temperature. N and $\mathrm{N_i}$ are the total column density and the column density of a given state i and $\mathrm{N_i}$ is determined directly from the measured extinction-corrected flux by

$$N_i = 4\pi \times flux(i)/(\Omega A(i) h\nu(i)) \tag{2}$$

where A(i) is the A-coefficient, $\nu(i)$ is the frequency of state i, Ω is the solid angle of the beam, and h is Planck's constant. Table 1 lists the values for the wavelength, rotational state, Einstein A-coefficient, energy, and statistical weight of the pure rotational levels of H_2 that we have observed with the *Spitzer* IRS.

In Figure 2 we present excitation diagrams from three different regions across the M51 strip. The excitation diagrams exhibit an ortho-to-para ratio (OPR) of 3 in the nuclear region. This is in agreement with the value of the OPR of the nuclear region determined by SINGS (Roussel et al. 2007). Outside the nucleus, the lower J (H_2 S(0) - H_2 S(3)) levels exhibit an OPR of 3. The H_2 S(4) measurement shows significant scatter in the excitation diagrams outside of the nuclear region of M51. This would indicate that the OPR is less than 3; however, due to the low signal-to-noise ratio of the H_2 S(4) map, we do not believe that the OPR determined from the H_2 S(4) intensity reflects the OPR of the warm H_2. The excitation-diagrams also exhibit a change in slope as a function of rotational level. This indicates that a continuous distribution of H_2 temperatures is being sampled within the beam.

Because the excitation diagrams shown in Figure 2 indicate that we are sampling a range of excitation-temperatures in different regions across the M51 strip, we assume that the H_2 exists in the form of two discrete components. We define these two components as a warm (T $= 100 - 300$ K) H_2 phase and a hot (T $= 400 - 1000$ K) H_2 phase. We determine the excitation-temperature and mass distribution of the hot (T$= 400 - 1000$ K) H_2 phase from the least squares fit to the H_2 S(2) $-$ H_2 S(5) lines in the excitation diagram. We determine the excitation-temperature and mass distribution of the warm (T $= 100 - 300$ K) H_2 phase from the least squares fit to the H_2 S(0) $-$ H_2 S(2) lines in the excitation diagram; however, because the warm and hot H_2 phases are inherently coupled, we subtract the the contribution of the hot H_2 from the warm H_2 in order to determine the warm H_2 excitation-temperature and mass (Higdon et al. 2006).

3.2.2. Warm and Hot H_2 *Mass Distributions*

In Figure 3 we present the warm (*left*) and hot (*right*) H_2 mass distributions across the M51 strip. Note that the non-rectangular shape of the strip is due to the offset between the SL and LL strips. Also note that the sizes of the plots of the warm and hot H_2 mass phases are different. The warm H_2 mass is determined from the H_2 S(0) $-$ H_2 S(2) maps of the H_2 emission across the entire strip. The hot H_2 mass is determined from the higher J rotational states for which the H_2 emission is not well-resolved across the strip. The warm H_2 mass peaks in the inner northwest spiral arm with 11 $M_\odot/pc^2$ warm H_2. The mass in the outer northwest and southeast spiral arms peaks toward the center of the spiral arms with 3.5 $M_\odot/pc^2$ warm H_2 and 1.0 $M_\odot/pc^2$ warm H_2 (in the northwest and southeast arms, respectively).

The peak in hot H_2 mass appears to be bimodal with a peak in the nucleus of the galaxy containing 0.24 $M_{\odot}/pc^2$ and a second peak that is interior to the inner spiral arm, also containing 0.24 $M_{\odot}/pc^2$. The hot H_2 mass in the spiral arms is only $\sim$ 20 - 30 % of the hot H_2 mass in the nucleus. We would like to note that in M51, we are sensitive to 0.40 $M_{\odot}/pc^2$ warm H_2 and 0.005 $M_{\odot}/pc^2$ hot H_2 within our beam.

3.2.3. Warm and Hot H_2 *Excitation-Temperature Distributions*

In Figure 4 we compare the warm H_2 mass distribution to the excitation-temperature. The gas is warmest in the nuclear region of M51 with the temperature ranging from 175 $-$ 190 K in the center of the galaxy. The gas is cooler within the spiral arms of M51 than in the inter-arm regions. The temperature in this spiral arm decreases from 175 K at the outer surface layers to 154 K in the most dense region of the arm indicating that the warm H_2 excitation-temperature is cooler at higher H_2 densities. In the outer northwest and southeast spiral arms (at 5 $-$ 6 kpc from the center of the galaxy each) molecular the gas excitation-temperature ranges from 150 K at the center to about 175 K near the edge of the spiral arms; again indicating that high density regions are cooler than low density regions.

The excitation-temperature distribution of the hot H_2 is shown in Figure 5 and reveals a different picture than the excitation-temperature distribution of the warm H_2. The excitation-temperature in the nuclear region ranges from 587 to 612 K. The excitation-temperature in the northwest inner spiral arm is the coolest at 538 K. The hottest excitation-temperatures are observed in the inter-arm regions where there is the least amount of H_2. In contrast, in the southeast inter-arm region, the excitation temperature is in excess of 900 K.

4. Discussion

4.1. Comparison to Previous Studies of Warm and Hot H_2 in Galaxies

Previous studies of pure rotational H_2 emission in galaxies have used aperture average spectra over the central regions of galaxies to derive the excitation temperature and mass of the warm and hot molecular gas phases within a galaxy (Rigopoulou et al. 2002; Higdon et al. 2006; Roussel et al. 2007). SINGS has studied molecular hydrogen in M51 and finds that within the central 330 arcsec^2, the excitation-temperature and mass of the warm (T = 100 − 300 K) H_2 phase are T = 180 K and $M_{warm} = 1.46 \times 10^6$ $M_\odot$, respectively (Roussel et al. 2007). Within the central 412 arcsec^2 of M51, we measure a warm H_2 excitation-temperature of 186 K and mass of 1.63×10^6 $M_\odot$, consistant with the SINGS to within 10 %. SINGS also measures the excitation-temperature of the hot phase (though they do not measure the mass in the hot phase) and find a hot H_2 excitation-temperature of 521 K. Over the nuclear region of M51, we measure an excitation-temperature of 584 K.

Rigopoulou et al. (2002) measured the H_2 mass in the hot phase and found that the warm-to-hot mass fraction varies between $5 \times 10^3 - 1 \times 10^6$ for Seyferts. This is significantly higher than the warm-to-hot mass fraction (Figure 6) than we measure within the central 412 arcsec^2 of M51, 14.8. To measure the hot H_2 mass, we use the H_2 S(2) − H_2 S(5) lines, whereas Rigopoulou et al. (2002) used the H_2 S(5) − H_2 S(7) lines. Thus, the hot H_2 phase that they measured is preferentially offset to higher H_2 excitation-temperatures and lower H_2 masses.

4.2. The Warm-to-Hot H_2 Mass Ratio

In Figure 6, we compare the warm H_2 mass distribution to the hot H_2 mass distribution. The warm H_2 mass distribution peaks at in the northwest inner spiral arm and the hot H_2

mass distribution peaks at in the nucleus and in the region interior to the northwest spiral arm. It is evident from the figure that the warm-to-hot H_2 mass ratio is not constant across the galaxy but is lowest in the nucleus of the galaxy (at 12) and increases to 170 and 136 in the southeast and northwest spiral arms, respectively. The differences between the warm and hot H_2 mass distributions and the variations in the morphology of M51 as a function of rotational energy level suggest different origins to the warm and hot H_2 phases and that the primary excitation mechanisms of the warm and hot H_2 phases differ.

In order to understand the H_2 excitation and where each excitation mechanism is dominant, we made comparisons of the H_2 line intensity and mass distributions to diagnostics of three excitation mechanisms: UV photons emitted in dense photon dominated regions (PDRs) and H II regions, shocks, and X-rays. We use CO ($J = 1 - 0$) emission to determine the location of the H_2 relative to locations dense PDRs, Hα imagery to identify H II regions (Scoville et al. 2001), [O IV](25.98 μm) line emission as a diagnostic of shocks (Schearer and Stasinska 1999), and the $0.5 - 10.0$ keV X-ray band to distinguish X-ray dominated regions (XDRs). The following section compares the H_2 mass distributions to CO (J = 1 - 0), Hα, [O IV], and X-ray emission.

4.3. Distinguishing the H_2 Excitation Mechanisms

4.3.1. H_2 Excitation by UV Photons from PDRs: Comparison of H_2 to CO Emission

In star-forming regions, H_2 exists within the PDR and deep into the molecular cloud. Owing to a low dissociation energy of 4.5 eV, H_2 formation generally does not occur within a PDR until the radiation field becomes sufficiently weak. Understanding H_2 in PDRs and implementing H_2 into photoionization codes has become the emphasis of many theoretical models. Recent advances in the CLOUDY photoionization code have included H_2 and modeled the structure of star-forming regions while treating the H II region and PDR as one continuous cloud (Shaw et al. 2005; Abel et al. 2005). Kaufman et al. (2006) used Starburst99/Mappings to model H_2 pure rotational line emission from PDRs to probe the conditions of dense PDRs in star-forming regions. They show that within galaxies, where the telescope beam size is generally kiloparsecs across, H_2 emission could serve to probe the surface layers of dense molecular clouds.

CO is found deep within a molecular cloud where the temperatures are too cold to excite H_2 emission. In these regions, CO is collisionally excited by the more abundant H_2 molecule. CO is connected to H_2 in star-forming regions because at the surface layers of the molecular clouds, H_2 is excited and CO emits dipole rotational lines due to heating by the ionizing radiation of newborn massive stars (Allen et al. 2004).

In Figure 7, we compare the warm (*left*) and hot H_2 (*right*) mass distributions to CO (J = 1 − 0) emission. The brightest CO emission is seen in the spiral arms where the greatest amounts of warm H_2 mass are also found. The most striking result is that in the inner spiral arms, we see that the CO is offset toward the nucleus from the warm H_2 mass. The offset between the peaks in CO and warm H_2 mass is $7\farcs2$ in the northwest spiral arms and $5''$ in the southeast spiral arms. We believe that these offsets are real with one possible explanation being that the H_2 is tracing the regions of active star-formation within the giant molecular associations.

We compare CO to the hot H_2 mass distribution (Figure 7, *right*) and we see that the hot H_2 mass is most abundant in the nuclear region, interior to the CO bright spiral arms. In northwest spiral arm, the hot H_2 mass is offset from the CO by $2\farcs6$. We believe that the offsets between the CO and the hot H_2 mass are real, however, they are likely due to the dominance of other excitation mechanisms (shocks or X-rays) in the nuclear region of M51.

In Figure 8, we compare the CO intensity to the H_2 S(0) − H_2 S(3) line intensity maps.

We see that the H_2 S(0) contours trace the CO spiral arms with one notable difference being that we detect H_2 S(0) emission far ($5 - 6$ kpc) from the nucleus of M51, where there is no CO detected. The H_2 S(1) $-$ H_2 S(3) contours also trace the CO spiral arms; however, within the spiral arms, the H_2 is not necessarily aligned with the CO. For example, in the comparison of H_2 S(3) to CO, we see that in the inner spiral arms, the H_2 contours trace the CO; however, within the northwest arm, we see that there is strong H_2 emission offset to the west by $9''.3$ from the bright CO emission in the same spiral arm. The offsets between the peaks in H_2 and CO emission are not systematic in any direction.

The CO intensity in the nucleus of the galaxy is much fainter than in the bright CO spiral arms. This is interesting because H_2 S(1) $-$ H_2 S(3) emission is brightest in the nucleus of M51 where H_2 emission from the higher J lines is likely due to more energetic processes such as shock excitation and X-rays (which we discuss in §4.3.3 and §4.3.4).

4.3.2. H_2 *Excitation by UV Photons from H II Regions: Comparison of* H_2 *to H*α *Emission*

H II regions are sites of recent massive star formation. They illuminate bright nebulae in distant galaxies and outline the spiral arms. H II regions emit prodigious amounts of UV radiation at energies ≥ 13.6 eV capable of exciting and ionizing H_2. Hα imagery is often used to identify and map H II regions in star-forming galaxies. Scoville et al. (2001) used Hα and Paα imagery to identify and characterize over 1,350 H II regions in M51.

In Figure 9, we compare the warm (*left*) and hot (*right*) H_2 mass distributions to Hα emission. In general, the warm and hot H_2 concentrations are not cospatial with the Hα emission regions in the spiral arms with the one exception being that the warm H_2 mass in the inner spiral arms appears to trace the Hα emission. The warm H_2 mass contours show that local peaks in H_2 mass are found within the dust lanes. An example of this is in the northwest spiral arms where we see the H_2 mass offset from the Hα spiral arms with local peaks being found in the dust lanes.

In Figure 10, we compare the H_2 S(0) $-$ H_2 S(3) line intensity maps to Hα emission. Comparison of the H_2 S(0) map to Hα reveals that the strongest H_2 emission in the northwest and southeast inner spiral arms is coincident with Hα emission; however, the other H_2 S(0) spiral arms show the strongest emission in the dust lanes, offset from the Hα spiral arms. The largest offsets are seen in the southwest spiral arm where the H_2 S(0) emission is offset from the Hα spiral arm by $\sim 15''$ (560 pc). H_2 S(1) emission appears to follow the dust lanes and the H_2 S(1) intensity subsides into the Hα spiral arms. H_2 S(2) and H_2 S(3) emission is also found in the dust lanes; however, there are instances (such as in the southeast spiral arm) where the H_2 emission appear to be found straddling the dust lane and Hα spiral arm.

These results are in contradiction to a previous study of rovibrational H_2 line emission in Seyfert galaxies by Quillen et al. (1999) who used *HST* NICMOS to map the H_2(1-0)S(1) (2.121 μm) and H_2(1-0)S(3)(1.957 μm) lines in 10 Seyfert galaxies. They found that the H_2 emission is generally coincident with Hα emission and near the dust lanes (though offset from them). One explanation for this could be that the rovibrational lines trace a much hotter (1000 $-$ 5000 K) molecular gas which can be found associated with H II regions whereas the cooler H_2 traced by the lowest pure rotational transitions is found in dense PDRs and molecular clouds associated with star forming regions.

4.3.3. H_2 *Excitation by Shocks: Comparison of* H_2 *to [O IV](25.89 μm) Emission*

The [O IV](25.89 μm) line can be excited in shocks (Schearer and Stasinska 1999), the stellar winds of massive Wolf-Rayet stars (Lutz et al. 1998), or by an active galactic nucleus (AGN)(Smith et al. 2004). Though the [O IV] line is bleneded with the [Fe II](25.99 μm) line in *Spitzer* IRS low resolution spectra, PAHFIT can deblend the two lines and in mapping the H_2 S(0) and H_2 S(1) line in the LL data cubes, we also mapped the [O IV] line.

In Figure 11, we compare the [O IV] intensity to the warm (*left*) and hot (*right*) H_2 disributions. The [O IV] emission is brightest in the nuclear region at 8.75×10^{-18} W/m^2 and the peak is coincident with the nuclear peak in the mass of the hot H_2. [O IV] emission subsides from the nucleus to the inner spiral arm by 50 %. We resolve weaker [O IV] emission within the warm and hot H_2 spiral arms. The [O IV] intensity in the spiral arms is a factor of ~ 6 lower in the spiral arms than the peak intensity found in the nucleus.

The [O IV] emission within the nuclear region of M51 is likely due to the weak Seyfert II nucleus (Ford et al. 1985) and is possibly associated with shocked gas from the outflows of the AGN. The peak of the [O IV] emission coincides with the nuclear peak in hot H_2 mass indicating that the hot H_2 phase in the nuclear region of the galaxy is AGN or shock heated. With 2.43×10^5 $M_\odot$ of hot H_2 in the central 0.58 kpc^2, it is unlikely that the hot H_2 is fueling the central AGN, but is excited by the AGN or shocks produced by it. In the nuclear region we observe a factor of 12 times greater warm H_2 mass. The warm H_2 mass is much greater within the spiral arms than within the nucleus and the warm-to-hot mass ratio is lowest in the nuclear region where the [O IV] intensity is greatest. In the nuclear region, shocks appear to be a more efficient means to excite the hot H_2 phase than the warm H_2 phase.

4.3.4. H_2 *Excitation by X-rays: Comparison of* H_2 *to X-ray Emission*

M51 has been extensively studied in X-rays by ASCA (Terashima et al. 1998), Newton XMM (Dewangan et al. 2005), and the Chandra X-ray Observatory (Terashima and Wilson 2001). These observations of M51 have revealed more than 80 X-ray sources. Candidates for these X-ray sources include neutron stars, black holes, supernova remnants (SN 1994I), and a low-luminosity AGN (Immler et al. 2002; Terashima and Wilson 2001). X-ray emission from the nuclear region of M51 has been studied by Terashima and Wilson (2001). They observe X-ray emission from the nucleus, the extranuclear cloud (XNC, to the south of the nucleus), and the northern loop. A radio jet has been observed connecting the nucleus of M51 to the XNC in 6 cm imagery (Crane and van der Hulst 1992). The jet emanates from the south of the elongated nucleus and is shock heating ISM.

In Figure 12, we compare the smoothed 0.5 - 10 keV band X-ray image to the warm (*left*) and hot (*right*) H_2 mass distributions. The 0.5 - 10 keV band has been smoothed to the resolution of the warm and hot H_2 mass distributions and the nucleus, XNC, and northern loop are indistinguishable in the smoothed image. X-ray emission is most intense from the nucleus and decreases into the northwest spiral arm that contains the greatest H_2 mass. There appears to be very little connection between the 0.5 - 10 keV X-ray band and the warm H_2 mass distribution.

The peak in X-ray emission is coincident with the hot H_2 mass peak. The most intense 0.5 - 10 keV X-ray emission originates from the nucleus and is oriented north-to-south, similar to the [O IV](25.89 μm) emission. The peak in X-ray emission is located within the peak in hot H_2 mass suggesting that X-rays play an important role in exciting the hot H_2 phase. While there is a correlation between X-ray emission and the hot H_2 phase, H_2 excitation by X-rays cannot be distinguished from H_2 excitation by shocks.

We further investigate X-ray excited H_2 emission in M51 by comparing the $0.5 - 10.0$ keV X-ray band to the H_2 S(2) $-$ H_2 S(5) line intensity maps (Figure 13). The H_2 S(2) $-$ H_2 S(5) line intensities all peak at the X-ray source within the nucleus. The X-ray source fits within the H_2 contours because the X-ray image resolution is slightly higher than the resolution of each of the H_2 maps.

The morphology of the nuclear H_2 emission appears to be correlated with the X-ray source. The H_2 S(2) intensity peaks around the X-ray nucleus and the intensity decreases to the south by 70 % in the southern XNC. The bar structure seen in the H_2 S(3) emission is aligned with X-ray emission from the nucleus, XNC, and northern loop. The H_2 S(3) intensity peaks between the X-ray nucleus and the XNC. To the north of the nucleus, the contours follow the X-ray loop. To the south of the nucleus (into the XNC), H_2 S(3) intensity decreases by 80 %. The H_2 S(4) and H_2 S(5) line intensities are highest in the nucleus which coincides with strong X-ray emission from the nucleus and XNC.

5. Conclusions

We have spectrally mapped a strip across M51 using the *Spitzer* IRS low resolution modules. We used the spatially resolved spectra to map H_2 S(0) $-$ H_2 S(5) line intensities across the strip. We find:

1. The morphology of H_2 emission in M51 varies with H_2 rotational level. H_2 S(0) emission is strongest in the spiral arms of the galaxy while the higher J transitions show the strongest emission towards the nucleus. The H_2 S(1) intensity is strongest in the nuclear region and in the northwest spiral arms, however, the peak in H_2 S(0) intensity in the northwest spiral arm is offset from the peak in H_2 S(0) intensity by $10\farcs2$. The H_2 S(2) and H_2 S(3) maps show H_2 emission in the nucleus, spiral arms, and inter-arm regions of M51

and bar structure aligned north-to-south is apparent in H_2 S(3) emission. H_2 S(4) and H_2 S(5) emission is resolved in the nuclear region of M51.

2. The different morphologies of H_2 emission in M51 indicate significant spatial variations in H_2 excitation-temperature and mass. Excitation diagrams reveal that the H_2 exists in a continuous distribution of temperatures across the galaxy. Using the low J lines to trace the warm (T = 100 − 300 K) H_2, we find that the warm H_2 excitation-temperature is highest in the nuclear region at 192 K and the warm H_2 mass peaks in the northwest inner spiral arm at a mass density of 11 $M_\odot/pc^2$. Using the higher J lines to trace the hot (T = 400 − 1000 K) H_2, we find that the hot H_2 excitation-temperature is lowest in the inner spiral arms (500 − 550 K) and increases to $\sim$ 600 K in the nucleus, where the largest hot H_2 mass densities are found to be 0.24 $M_\odot/pc^2$.

3. The warm and the hot H_2 mass distributions are not cospatial and the warm-to-hot mass ratio varies across M51. The hot mass distribution shows two peaks, one in the nucleus of M51 and one located interior to the northwest inner spiral arm of M51. The warm mass distribution peaks in the northwest spiral arm and is offset from the hot mass peak by $11''.4$. The warm-to-hot mass ratio varies across the galaxy with the ratio being $\sim$ 15 in the nucleus and increasing to $>$ 100 in the spiral arms. Variations in the warm-to-hot H_2 mass ratio and differences in the morphology of the H_2 emission across M51 indicate that the primary excitation mechanism differs for the warm and hot H_2 mass phases as a function of location within the galaxy.

4. CO emission is offset from the warm H_2 mass in the inner spiral arms of M51. These apparent offsets are real and are possibly associated with the regions of active star formation within the molecular clouds. In the spiral arms, the H_2 S(0) − H_2 S(3) contours

trace the CO; however, within the spiral arms, the peaks in H_2 can be offset from the peaks in CO intensity. In the nucleus, the H_2 S(1) − H_2 S(3) lines are brightest and the CO intensity is a factor of ∼ 2.5 weaker than in the spiral arms suggesting that H_2 emission from the higher J lines is excited by shocks of X-rays.

5. Comparing the distributions of H_2 to Hα reveals that the warm and hot H_2 mass is found in the dust lanes rather than at or around the Hα emission regions with the one exception being that the warm H_2 mass in the inner spiral arms is coincident with bright Hα emission. This is in contradiction to previous studies of spatially resolved rovibrational H_2 line emission in Seyferts that found the H_2 emission to be coincident with the Hα emission.

6. The peaks in [O IV](25.89 μm) intensity and and X-ray intensity are both coincident with the peak in hot H_2 mass in the nucleus of M51 suggesting that the hot H_2 in the nucleus is primarily excited by the AGN, shocks (possibly associated with the AGN), or X-rays associated with the AGN. The spatial distributions of the [O IV] emission and X-ray surface brightness are very similar, but a primary excitation mechanism (shocks or X-rays) of the hot H_2 mass phase cannot be distinguished. Further comparison of the H_2 S(2) − H_2 S(5) intensity maps to the X-ray surface brightness reveal that the nuclear H_2 emission is associated with X-rays and the bar structure apparent in the H_2 S(3) map is aligned with the nucleus, XNC, and northern loop.

The author graciously acknowledges the Spitzer Science Center Spitzer Visiting Graduate Student Fellowship program and committee for providing support for this research. The author would like to specifically acknowledge the program coordinators, Phil

Appleton and Alberto Noriega-Crepso. The author would also like to thank JD Smith for swift responses to questions about PAHFIT and CUBISM and Nicolas Flagey for productive discussions about PAHFIT. Partial support for the completion and preparation for publication of this study by the author was provided by AURA grant GO10822.1 to Rice University.

Facilities: Spitzer Science Center (SSC), Spitzer Space Telescope (SST), Berkely-Illinois-Maryland Array (BIMA).

REFERENCES

Aalto, S., Huttemeister, S., Scoville, N.Z., and Thaddeus, P., 1999, AJ, 522, 165

Abel, N.P., Ferland, G.J., Shaw, G., and van Hoof, P.A.M., 2005, ApJS, 161, 65

Allen, R.J., Heaton, H.I., and Kaufman M.J., 2004, ApJ, 608, 314

Blitz, L., 1995, SSR, 684

Calzetti, D. et al., 2005, ApJ, 633, 871

Carpenter, J.M. and Sanders, D.B., 1998, AJ, 116, 1856

Crane, P.C. and van der Hulst, J.M., 1992, AJ, 103, 1146

Dewangn, G.C., Griffiths, R.E., Choudhury, M., Miyaji, T., and Schurch, N.J., 2005, ApJ, 635, 198

Ford, H.C., Crane, P.C., Jacoby, G.H., Lawrie, D.G., and van der Hulst, J.M., 1985, ApJ, 293, 132

Helfer, T.T., Thornley, M.D., Regan, M.W., Wong, T., Sheth, K., Vogel, S.N., Blitz, L., and Bock, D.C.J., 2003, ApJS, 145, 259

Higdon, S.J.U., Armus, L., Higdon, J.L., Soifer, B.T., and Spoon, H.W.W., 2006, ApJ, 648, 323

Houck, J.R. et al., 2004, ApJS, 145, 18

Immler, S., Wilson, A.S., and Terashima, Y., 2002, ApJ, 573, L27

Kaufman, M.J., Wolfire, M.G., and Hollenbach, D.J., 2006, ApJ, 644, 283

Lord, S.D. and Young, J.S., 1990, ApJ, 356, 135

Lutz, D., Kunze, D., Spoon, H.W.W., and Thornley, M.D., 1998, A&A, 333, L75

Kennicutt, R.C. et al., 2003, PASP, 115, 928

Kenny, J.D.P. and Lord, S.D., 1991, ApJ, 381, 118

Matsushita, S. et al., 2004, ApJ, 616, L55

Neufeld, D.A., Melnick, G.J., and Harwit, M., 1998, ApJ, 506, L75

Neufeld, D.A., Melnich, G.J., Sonnentrucker, P., Bergin, E.A., Green, J.D., Kim, K.H., Watson, D.M., Forrest, W.J., and Pipher, J.L., 2006, ApJ, 649, 816

Palumbo, G.G.C., Fabbiano, G., Fransson, C., and Trinchieri, G., 1985, ApJ, 298, 259

Quillen, A.C., Alonso-Herrero, A., Rieke, M.J., Rieke, G.H., Ruiz, M., Kulkarni, V., 1999, ApJ, 527, 696

Regan, M.W., Thornley, M.D., Helfer, T.T., Sheth, K., Wong, T., Vogel, S.N., Blitz, L., and Bock, D.C.J., 2001, ApJ, 561, 218

Rigopoulou, D., Kunze, D., Lutz, D., Genzel, R., and Moorwood, A.F.M., 2002, A&A, 389, 374

Roussel, H. et al., 2007, in press

Schaerer, D. and Stasinska, G., 1999, A&A, 345, L17

Scoville, N.Z. and Young, J.S., 1983, AJ, 265, 148

Scoville, N.Z., Yun, M.S., Armus, L., and Ford, H., 1998, ApJ, 493, L63

Scoville, N.Z., Polletta, M., Ewald, S., Stolovy, S.R., Thompson, R., and Rieke, M., 2001, AJ, 122, 3017

Shaw, G., Ferland, G.J., Abel, N.P., Stancil, P.C., and van Hoof, P.A.M., 2005, ApJ, 624, 794

Sheth, K., Regan, M.W., Vogel, S.N., and Teuben, P.J., 2000, ApJ, 532, 221

Sheth, K., Vogel, S.N., Regan, M.W., Tueben, P.J., Harris, A.I., and Thornley, M.D., 2002, AJ, 124, 2581

Sheth, K., Vogel, S.N., Regan, M.W., Thornley, M.D., and Teuben, P.J., 2005, ApJ, 632, 217

SINGS: The Spitzer Infrared Nearby Galaxies Fouth Data Delivery, May 2006.

Smith, J.D.T. et al., 2004, ApJS, 154, 199

Smith, J.D.T. et al., 2007, ApJ, 656, 770

Terashima, Y., Ptak, A., Fujimoto, M.I., Kunieda, H., Makishima, K., and Sherlemitsos, P.J., 1998, ApJ, 496, 210

Terashima, Y. and Wilson, A.S., 2001, ApJ, 560, 139

Tully, R.B. 1988, Nearby Galaxies catalog (Cambridge:Cambridge University Press)

Vogel, S.N., Kulkarni, S.R., and Scoville, S.Z., 1988, Nature, 334, 402

Young, J.S. and Devereux, N.A., 1991, ApJ, 373, 414

Young, J.S. and Scoville, N.Z., 1991, ARA&A, 29, 581

This manuscript was prepared with the AAS LaTeX macros v5.2.

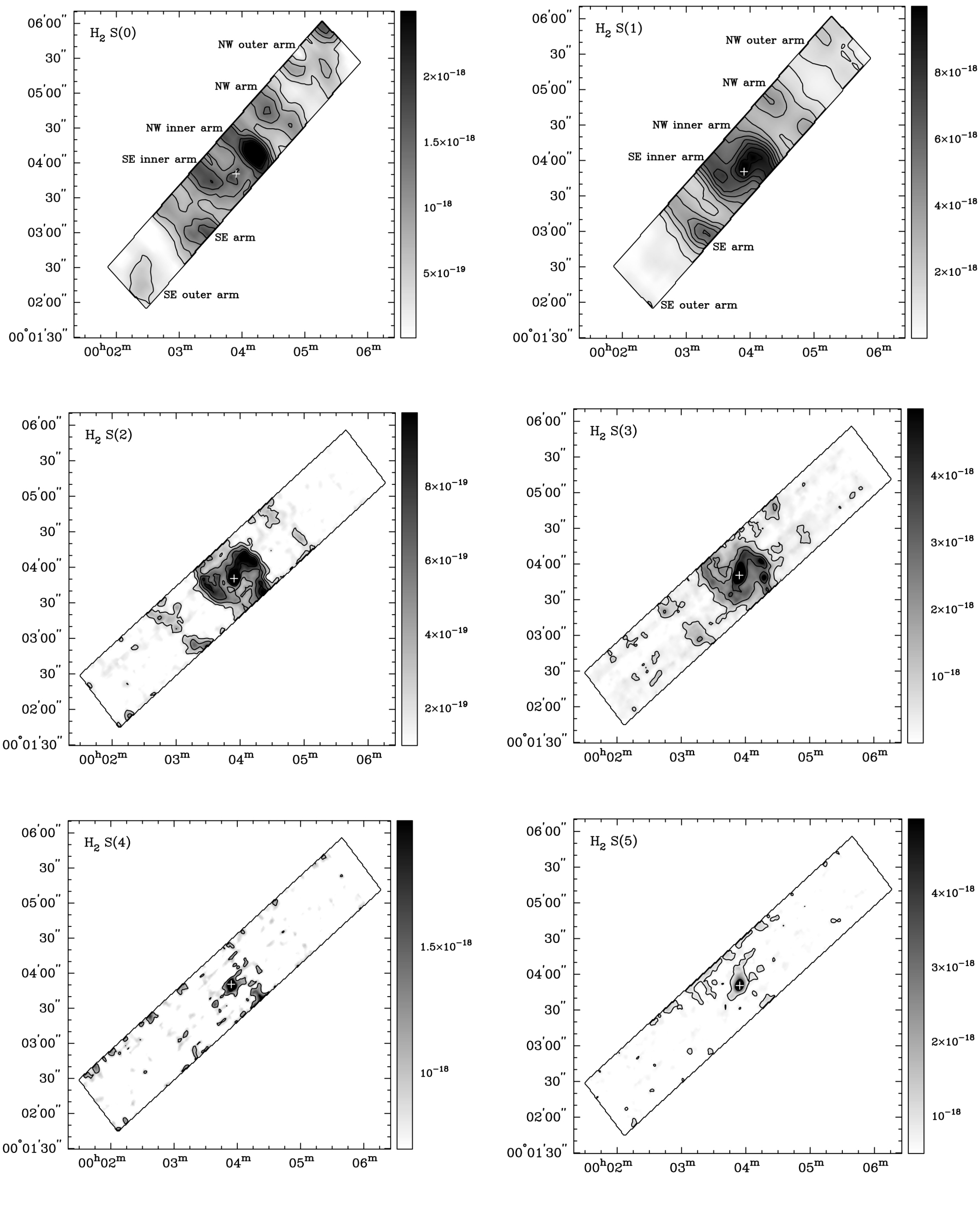
H$_2$ S(0)
NW outer arm
NW arm
NW inner arm
SE inner arm
SE arm
SE outer arm
H$_2$ S(1)
H$_2$ S(2)
H$_2$ S(3)
H$_2$ S(4)
H$_2$ S(5)

Fig. 1.— Maps of the H_2 S(0) (*top left*), H_2 S(1) (*top right*), H_2 S(2) (*middle left*), H_2 S(3) (*middle right*), H_2 S(4) (*bottom left*), and H_2 S(5) (*bottom right*) intensity across the SL and LL strips that we mapped with the Spitzer IRS. The H_2 S(0) and H_2 S(1) maps are created from the LL data cubes. The H_2 S(2), H_2 S(3), H_2 S(4), and H_2 S(5) maps are created from the SL data cube. The grey-scale is in units of W/m^2. Contour levels are at 2.9 $\times$ 10^{-18}, 2.2 $\times$ 10^{-18}, 1.8 $\times$ 10^{-18}, 1.5 $\times$ 10^{-18}, 1.1 $\times$ 10^{-18}, 7.3 $\times$ 10^{-19}, and 3.7 $\times$ 10^{-19} W/m^2 for H_2 S(0); 9.6 $\times$ 10^{-18}, 8.6 $\times$ 10^{-18}, 7.5 $\times$ 10^{-18}, 6.4 $\times$ 10^{-18}, 5.4 $\times$ 10^{-18}, 4.3 $\times$ 10^{-18}, 3.2 $\times$ 10^{-18}, 2.1 $\times$ $10^{-18}$and 1.1 $\times$ 10^{-18} W/m^2 for H_2 S(1); 1.1 $\times$ 10^{-18}, 8.9 $\times$ 10^{-19}, 6.7 $\times$ 10^{-19}, 4.4 $\times$ 10^{-19}, and 2.2 $\times$ 10^{-19} W/m^2 for H_2 S(2); 1.21 $\times$ 10^{-17}, 9.4 $\times$ 10^{-18}, 6.7 $\times$ 10^{-18}, 4.0 $\times$ 10^{-18}, and 1.3 $\times$ 10^{-18} W/m^2 for H_2 S(3); 2.0 $\times$ $10^{-18}$and 1.0 $\times$ 10^{-18} W/m^2 for H_2 S(4); 7.3 $\times$ 10^{-18}, 4.0 $\times$ 10^{-18}, and 8.0 $\times$ 10^{-19} W/m^2 for H_2 S(5). The vertical axis is the right ascension and the horizontal axis is the declination. Note that in all of the maps, north is up and east is to the left. The different spiral arm regions are labeled on the H_2 S(0) and H_2 S(1) maps in order to aid in discussing the molecular gas morphologies. The box around the intensity maps represents the SL or LL strip that we mapped.

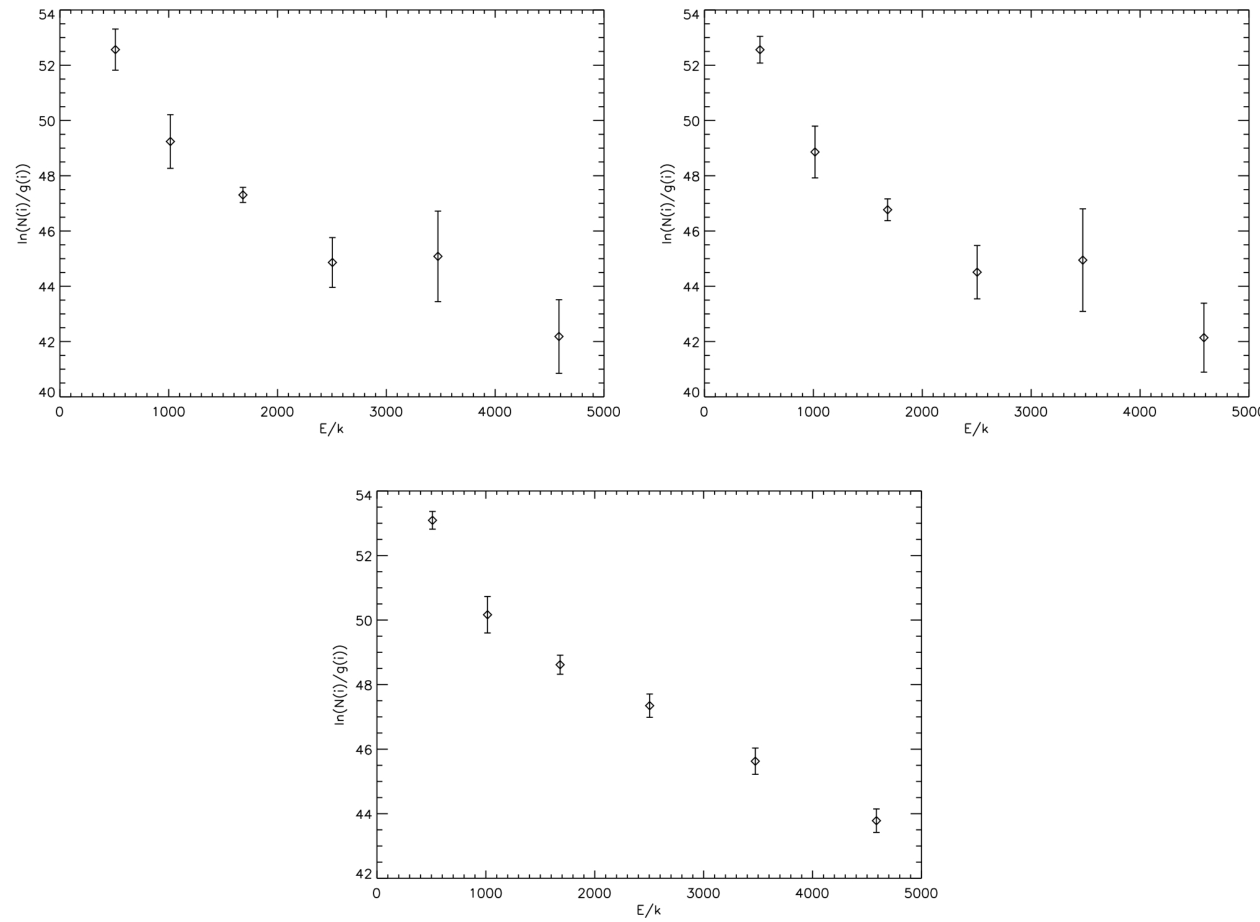

Fig. 2.— Excitation diagrams taken from 3 different regions along the M51 strip. The top two excitation diagrams are taken from regions within the southeast and northwest spiral arms that are 10.″2 in diameter (1.13×10^5 pc^2) and centered at (RA, Dec) of (202.45, 47.21) and (202.49, 47.18), respectively. The excitation diagram at the bottom is taken from from the nuclear region. The aperture is 10.″2 in diameter (1.13×10^5 pc^2), centered at (RA, Dec) of (202.47, 47.19).

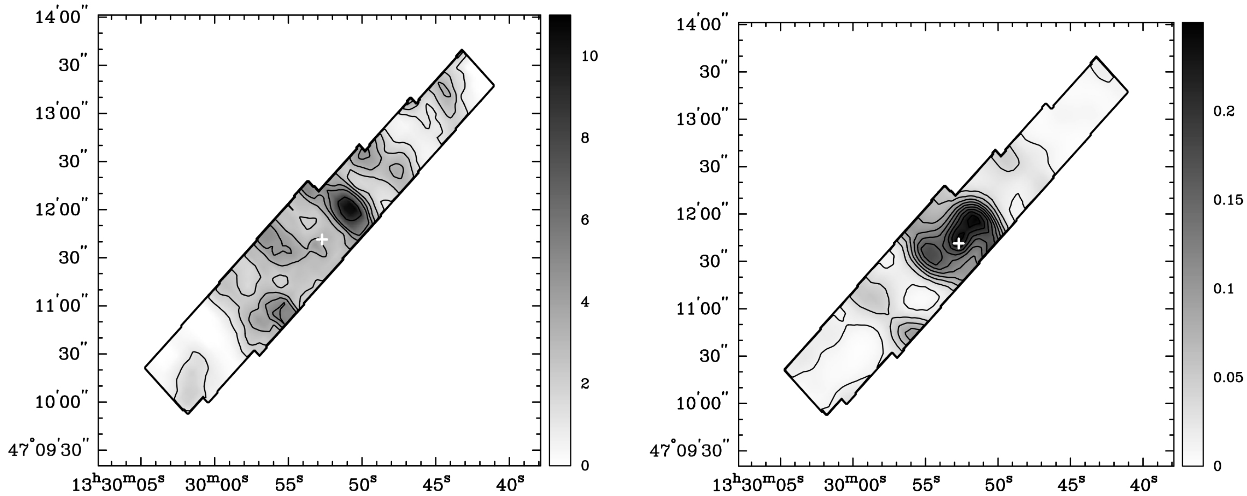

Fig. 3.— Shown are the warm (T = 100 − 300 K) H_2 (*left*) and hot (T = 400 − 1000 K) H_2 (*right*) mass distributions. The mass distributions are in units of $M_\odot/pc^2$. Contours are overplotted for clarity. The warm H_2 mass contour levels are at 8.85, 5.55, 4.43, 3.32, 2.21, and 1.10 $M_\odot/pc^2$. The hot H_2 contour levels are at 10 % of 0.25 $M_\odot/pc^2$. The hot H_2 mass distribution is derived from the fit to the H_2 S(2) − H_2 S(5) lines and the warm H_2 mass distribution is derived from the fit to the H_2 S(0) − H_2 S(2) lines, corrected for the contribution of the hot H_2 mass phase.

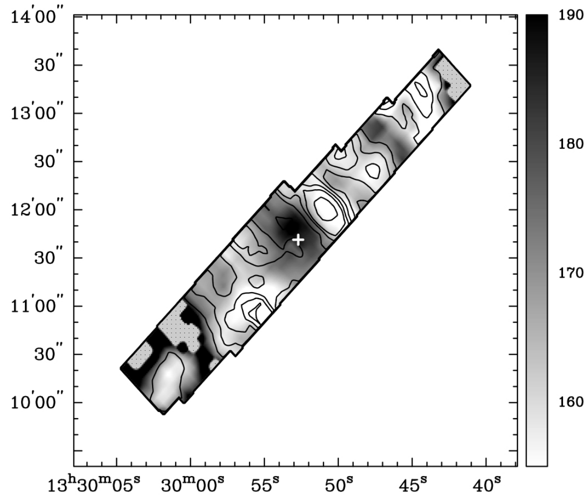

Fig. 4.— The warm (T = 100 − 300 K) H_2 mass distribution compared to the warm H_2 excitation-temperature. The warm H_2 excitation-temperature and mass distributions are derived from the fit to the excitation diagrams across the strip for the H_2 S(0) − H_2 S(2) lines, corrected for the contribution of the hot (T = 400 − 1000 K) H_2 phase. Mass density contour levels are at 8.85, 5.55, 4.43, 3.32, 2.21, and 1.10 $M_\odot/pc^2$ (same as in Figure 3). The grey-scale represents the excitation-temperature distribution (in units of Kelvin). The non-rectangular shape to the map is due to the slight offset of the *Spitzer* IRS SL strip relative to the LL strip.

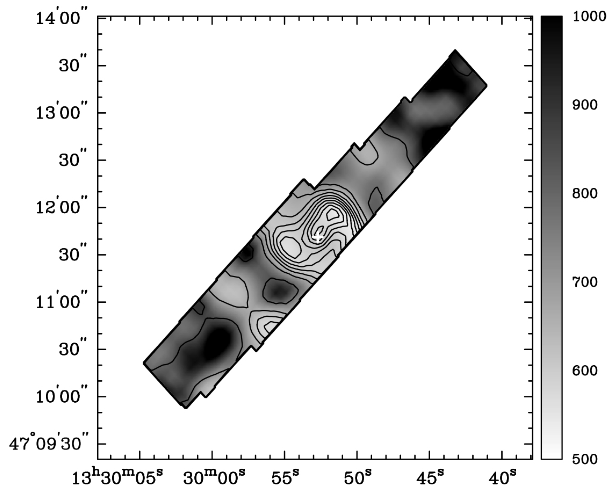

Fig. 5.— The hot (T = 400 − 1000 K) H_2 mass distribution compared to the hot H_2 excitation-temperature. The hot H_2 excitation-temperature and mass distributions are derived from the fit to the excitation diagrams across the strip for the H_2 S(2) − H_2 S(5) lines. Mass density contour levels are at 10% of 0.25 $M_\odot/pc^2$ (same as in Figure 3). The grey-scale represents the excitation-temperature distribution (in units of Kelvin).

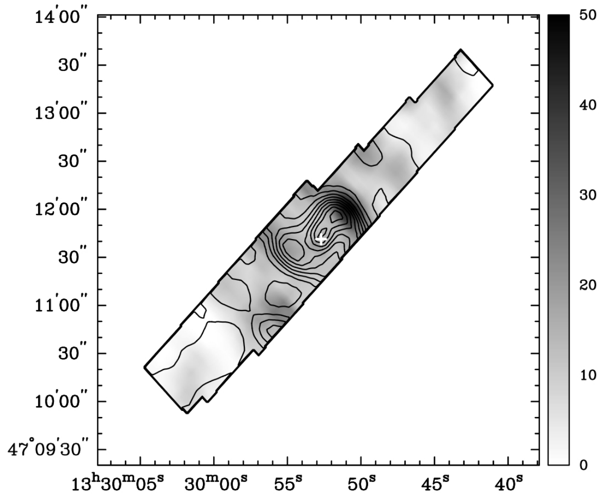

Fig. 6.— The warm (T = 100 − 300 K) H_2 mass (in grey-scale) compared to the hot (T = 400 − 1000 K) H_2 mass (in contours). Contours levels for the hot H_2 mass distribution are at 10% of the maximum mass density 0.25 $M_\odot/pc^2$. The grey-scale is in units of $M_\odot/pc^2$.

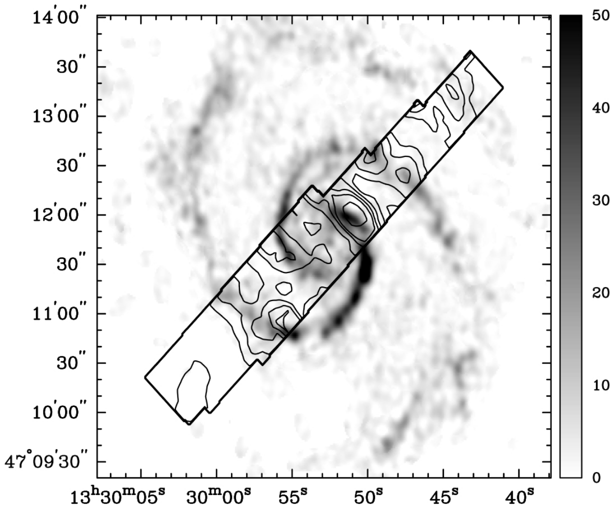

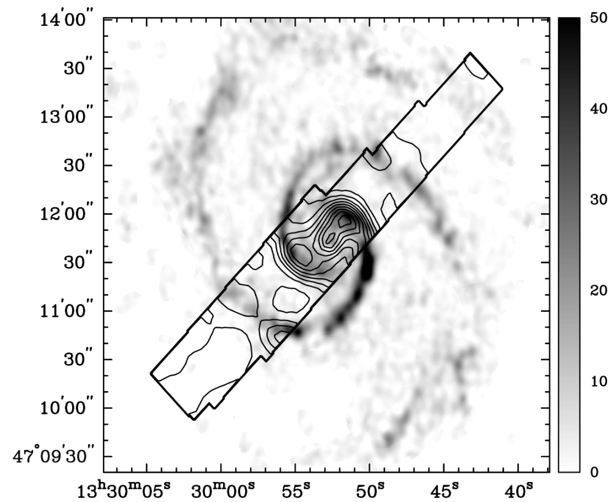

Fig. 7.— *Left*: Comparison of CO intensity (in grey-scale) to the warm (T = 100 − 300 K) H_2 mass (in contours). The CO intensity is in units of Jy beam s^{-1}. The warm H_2 mass contours are the same as in Figures 3 and 4. *Right*: Comparison of CO intensity (in grey-scale) to the hot (T = 400 − 1000 K) H_2 mass (in contours). The CO intensity is in units of Jy beam s^{-1}. The hot H_2 mass contours are the same as in Figures 3 and 5.

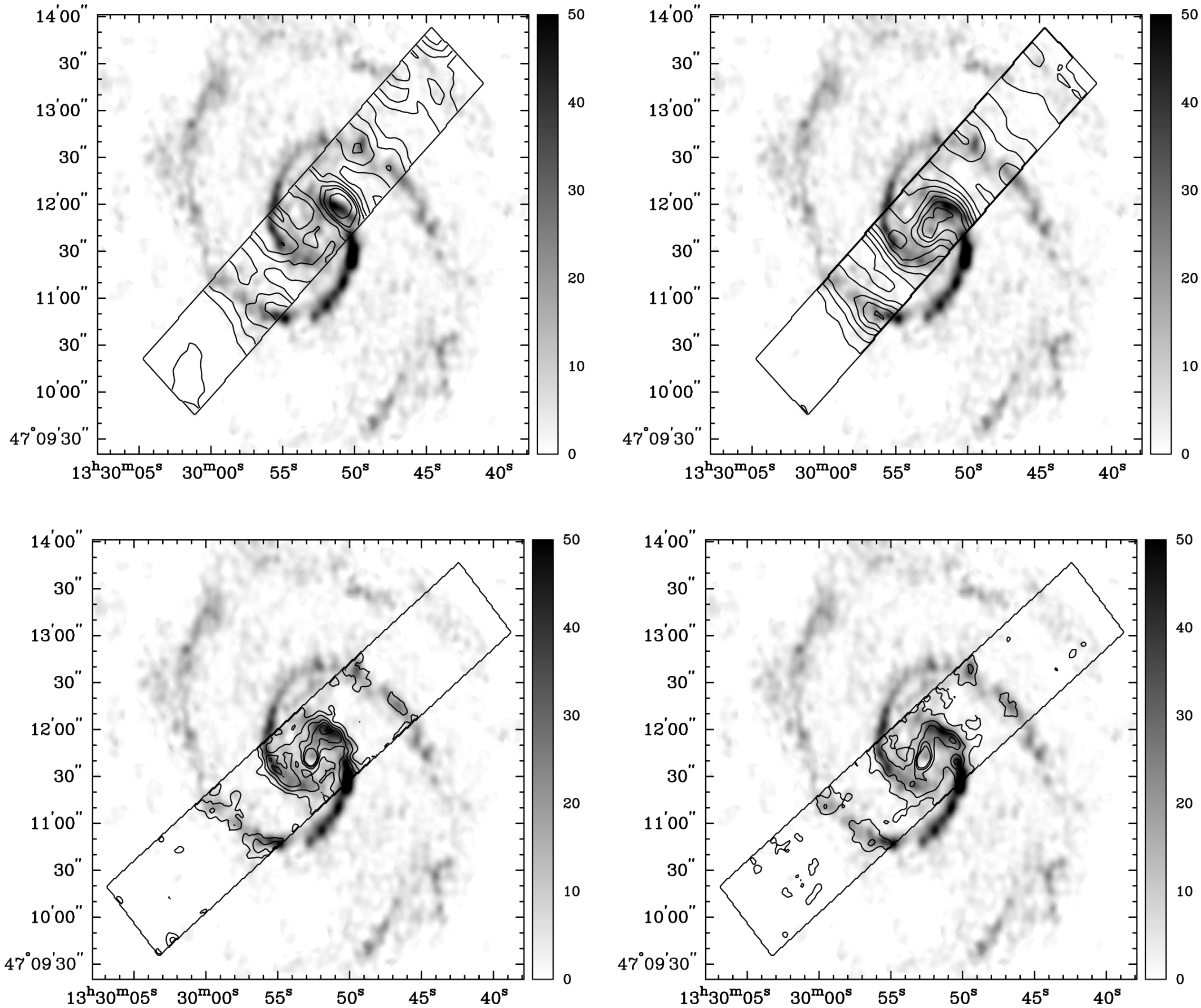

Fig. 8.— Comparison of the CO emission to the H_2 S(0) (*top left*), H_2 S(1) (*top right*), H_2 S(2) (*bottom left*), and H_2 S(3) (*bottom right*) emission. The CO emission maps are in units of Jy beam s^{-1}. Contour levels for H_2 S(0), H_2 S(1), H_2 S(2), and H_2 S(3) are the same as in Figure 1.

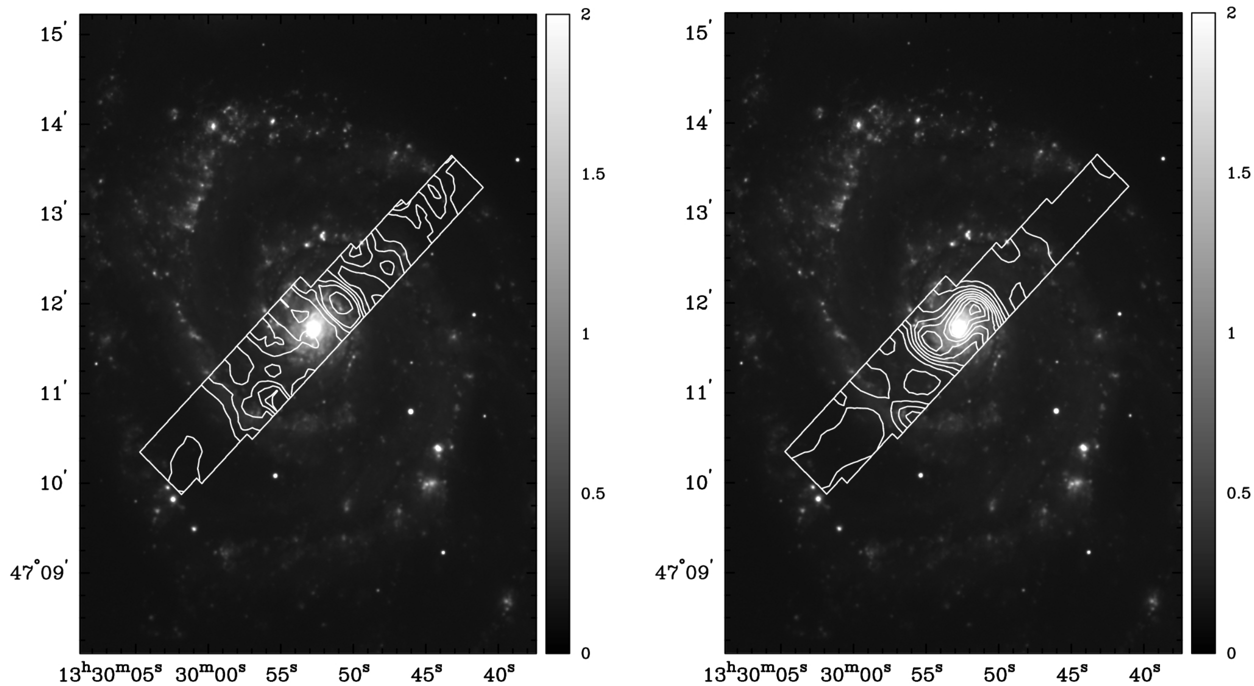

Fig. 9.— *Left*: Comparison of Hα (in grey-scale) to the warm (T = 100 − 300 K) H_2 mass (in contours). The Hα image is in units of counts/sec. The warm H_2 mass contours are the same as in Figures 3 and 4. *Right*: Comparison of Hα (in grey-scale) to the hot (T = 400 − 1000 K) H_2 mass (in contours). The Hα image is in units of counts/sec. The hot H_2 mass contours are the same as in Figures 3 and 5.

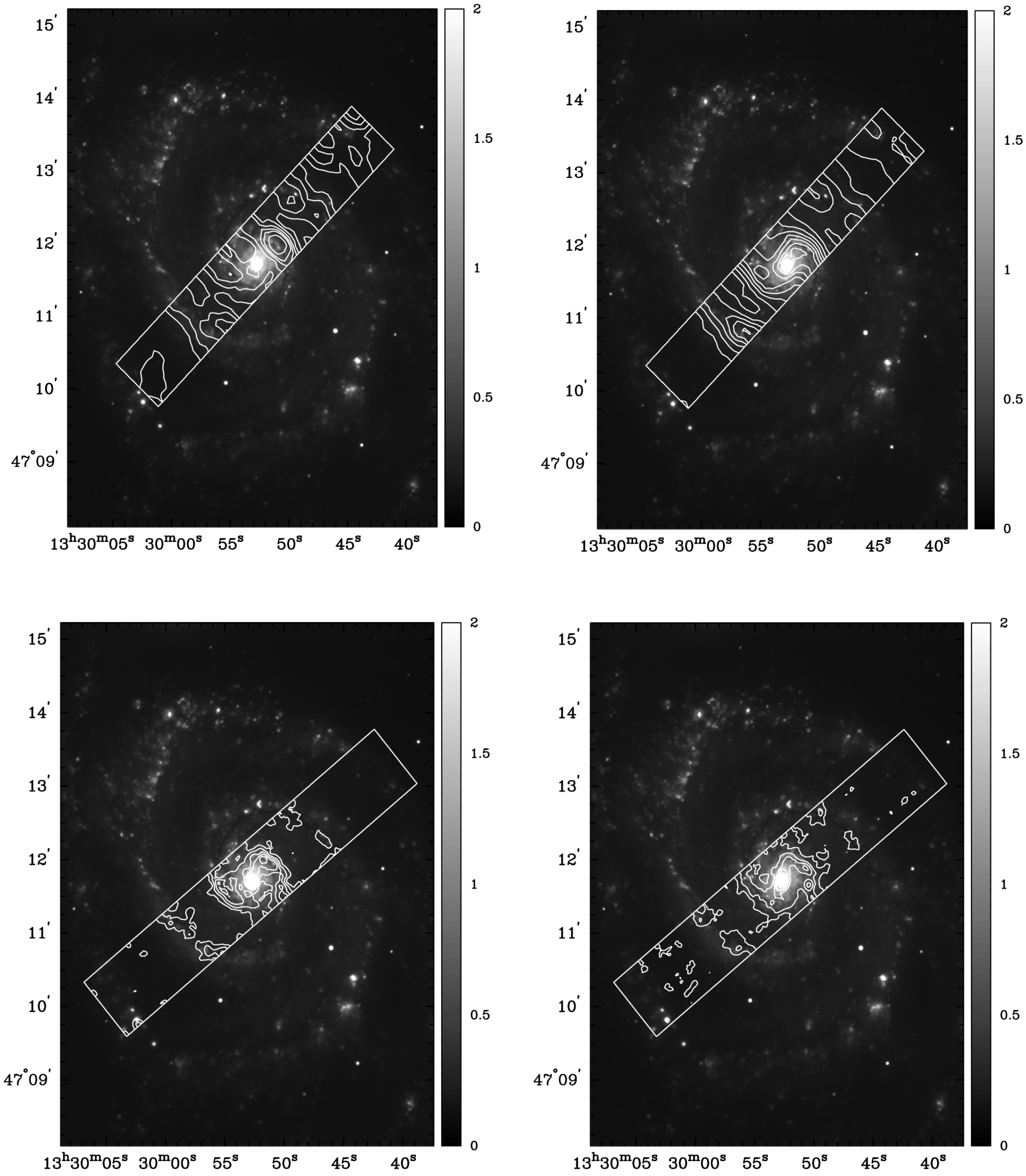

Fig. 10.— Comparison of Hα emission to the H_2 S(0) (*top left*), H_2 S(1) (*top right*), H_2 S(2) (*bottom left*), and H_2 S(3) (*bottom right*) emission. The Hα image is in units of counts/s. Contour levels for H_2 S(0), H_2 S(1), H_2 S(2), and H_2 S(3) are the same as in Figure 1.

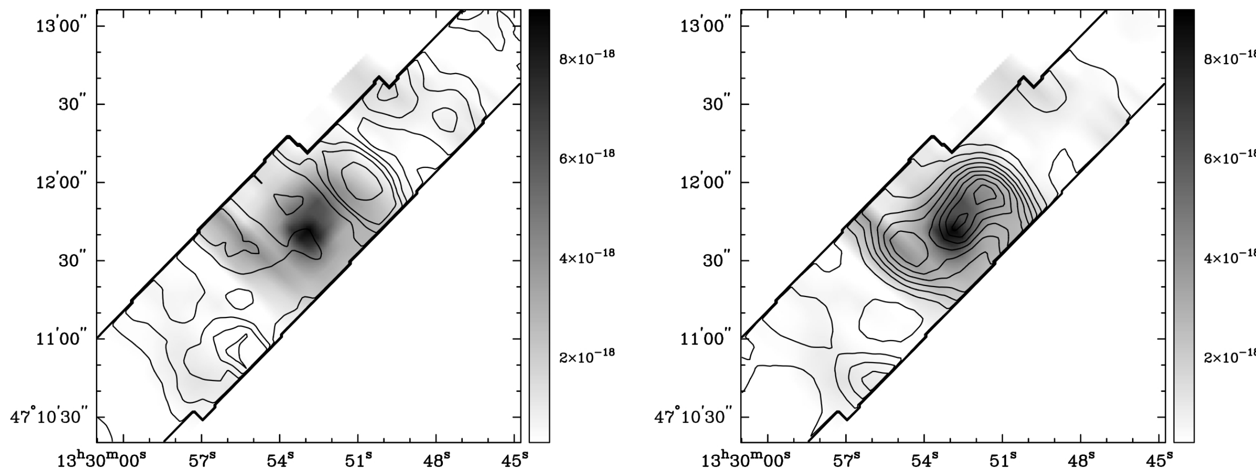

Fig. 11.— *Left*: Comparison of the [O IV](25.89 μm) emission (in grey-scale) to the warm (T = 100 K - 300 K) H_2 mass distribution (in contours). Hot H_2 mass contours are the same as in Figures 3 and 4. *Right*: Comparison of the [O IV](25.89 μm) emission (in grey-scale) to the hot (T = 400 - 1000 K) H_2 mass distribution (in contours). Hot H_2 mass contours are the same as in Figures 3 and 5. The [O IV](25.89 μm) emission is in units of W/m^2.

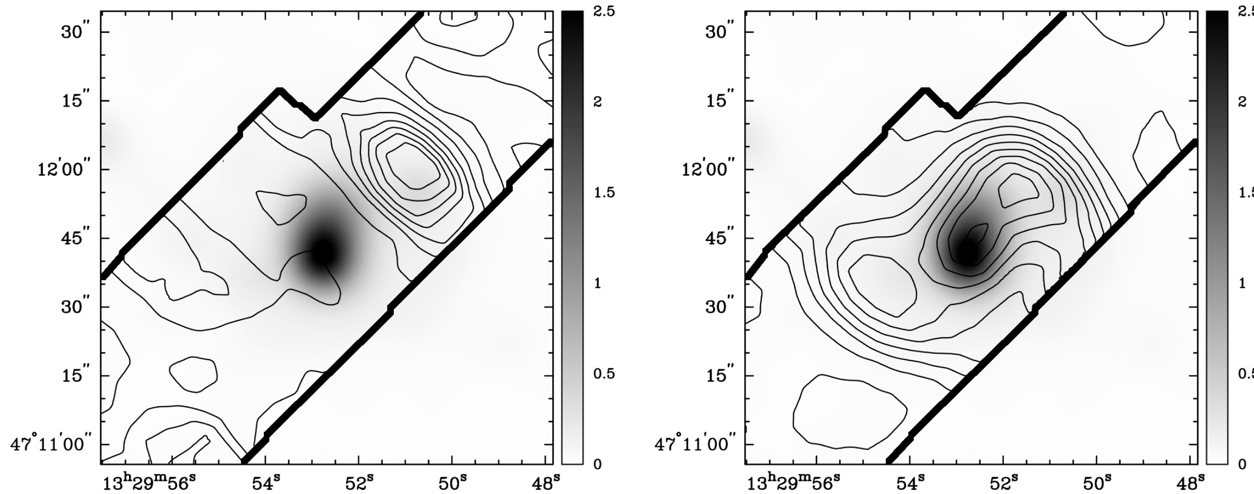

Fig. 12.— *Left*: Comparison of the smoothed 0.5 − 10 keV X-ray emission band (in grey-scale) to the warm (T = 100 − 300 K) H_2 mass distribution (in contours). The X-ray image has been smoothed to the same resolution as the warm H_2 mass map. X-ray emission is in units of counts. H_2 mass contours are the same as in Figures 3 and 4. *Right*: Comparison of the smoothed 0.5 − 10 keV X-ray emission band (in grey-scale) to the hot (T = 400 − 1000 K) H_2 mass distribution (in contours). The H_2 mass distribution contours are the same as in Figures 3 and 5.

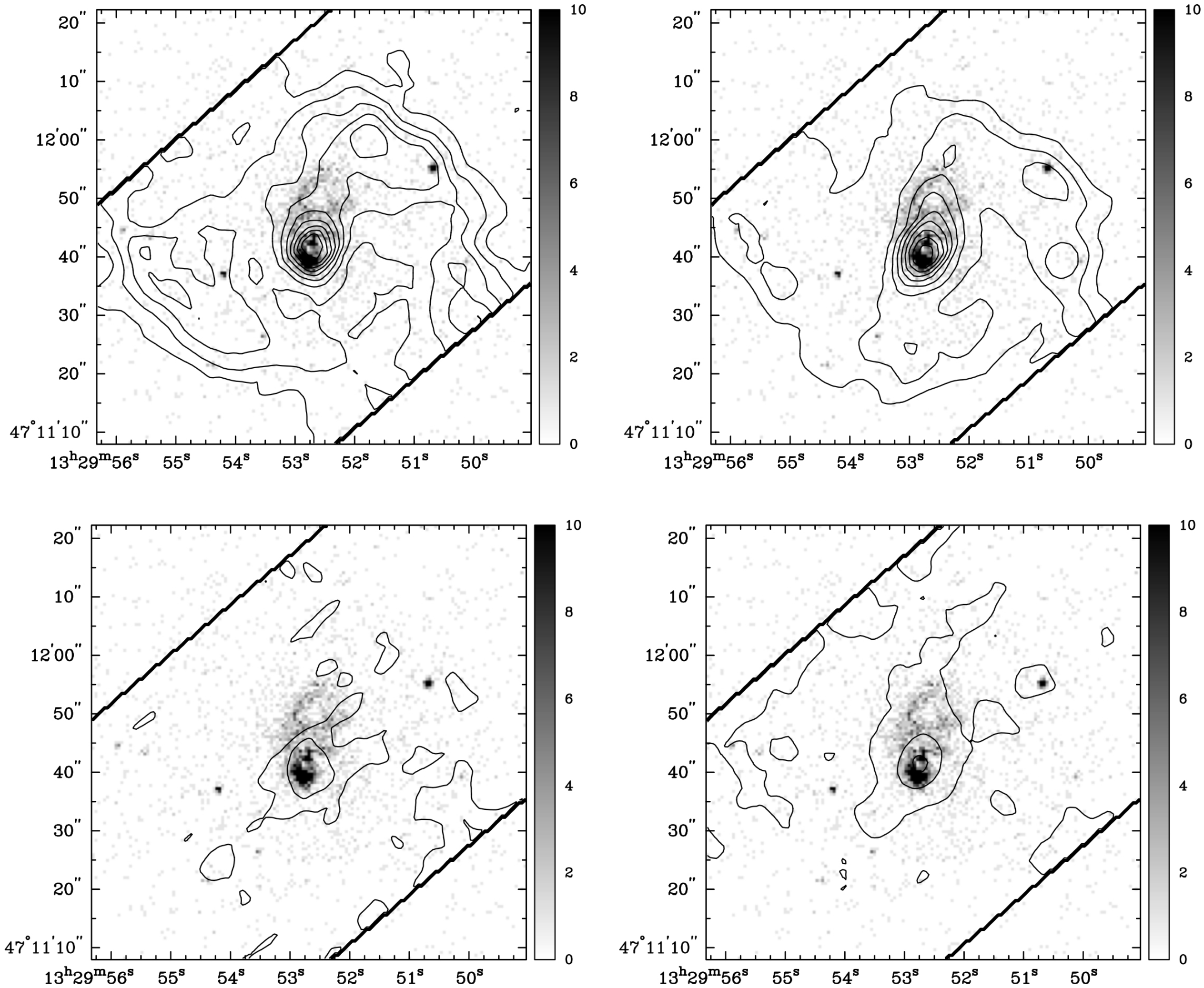

Fig. 13.— Comparison of the 0.5 − 10 keV X-ray emission band (in grey-scale) to the H_2 S(2) (*top left*), H_2 S(3) (*top right*), H_2 S(4) (*bottom left*), and H_2 S(5) (*bottom right*) emission in the nuclear region of M51. X-ray emission is in units of counts. The H_2 S(2) and H_2 S(3) emission contours are at 10 % of their peak values (2.20×10^{-18} and 1.35×10^{-17} W/m^2, respectively). The H_2 S(4) contours are at 2.0×10^{-18} and 1.0×10^{-18} W/m^2 and the H_2 S(5) contours are at 7.3×10^{-18}, 4.0×10^{-18}, and 8.0×10^{-19} W/m^2.

Table 1. H_2 Parameters

Transition	Wavelength (μm)	Rotational State (J)	Energy (E/k)	A (s^{-1})	Statistical Weight (g)
H_2(0-0)S(0)	28.22	2	510	2.94×10^{-11}	5
H_2(0-0)S(1)	17.04	3	1015	4.76×10^{-10}	21
H_2(0-0)S(2)	12.28	4	1682	2.76×10^{-9}	9
H_2(0-0)S(3)	9.66	5	2504	9.84×10^{-9}	33
H_2(0-0)S(4)	8.03	6	3474	2.64×10^{-8}	13
H_2(0-0)S(5)	6.91	7	4586	5.88×10^{-8}	45

Note. — The statistical weight (g) is $(2J+1)(2I+1)$ where I equals 1 for odd J transitions (ortho transitions) and I equals 0 for even J transitions (para transitions).